Int. J. Appl. Ceram. Technol., ■■ [■■] 1–9 (2010)
DOI:10.1111/j.1744-7402.2009.02484.x

International Journal of
Applied Ceramic TECHNOLOGY
Ceramic Product Development and Commercialization

Properties of Slip-Cast and Pressureless-Sintered ZrB_2–SiC Composites

Valentina Medri,* Claudio Capiani, and Alida Bellosi

ISTEC-CNR, National Research Council, Institute of Science and Technology for Ceramics, 64, I-48018 Faenza, Italy

In view of the perspective to produce near-net shapes of ultra-refractory ceramics, ZrB_2–SiC composite were produced by slip casting on plaster mould and pressureless sintered at 2150°C with a holding time of 120 min, using silicon nitride as a sintering aid. After sintering, slip-cast samples reached a very high relative density over 98%, while for comparison, the density of cold isostatic pressed samples was about 94%. Traces of the formation of secondary phases such as B_4C, graphite, and BN were found in all samples, while no grain boundary phases were revealed. RT flexural strength of as-sintered slip cast bars was affected by the presence of an external porous layer of coarse ZrB_2 particles, while at 1500°C the flexural strength increased, as a glassy layer sealed the superficial defects. Because of the absence of softening grain boundary phases, subcritical crack growth did not occur during high-temperature strength tests.

Introduction

Zirconium diboride is a material of particular interest because of the excellent and unique combination of high melting point, high electrical, and thermal conductivity, chemical inertness against molten metals or nonbasic slags, and superb thermal shock resistance.[1] These properties make it an attractive candidate for ultra-high-temperature applications where corrosion-wear-oxidation resistance is demanded.[2] Actually as ultra-high-temperature ceramics, ZrB_2-based materials attract strong interest for application in the aerospace industry: hypersonic reentry vehicles, leading edges, nose caps, rocket nozzle inserts, and air-augmented propulsion system components.

Generally, pressure-assisted sintering techniques at temperatures >1800°C are required to achieve complete densification of ZrB_2-based materials. However, this limits the possibility to produce complex shapes, because the brittleness and high hardness of these materials require expensive diamond machining to manu-

*valentina.medri@istec.cnr.it

facture net shapes from pieces with simple geometrical shapes. Besides, the electrical conductivity of ZrB_2 permits the production of complex-shaped parts by electrical discharge machining, but this technique induces the formation of a 5 μm thick slag on the external surfaces, which results in surface flaws. For this reason, pressureless sintering would be advantageous for the productions of near-net shape components, provided that a suitable forming technique is set up.

Pressureless densification up to 98% has been reported for ZrB_2-based materials; the sintering temperature ranges between 1850°C and 2250°C with a dependence on sintering aids (Mo, WC, and B_4C) or secondary phases, while uniaxial pressing and/or cold isostatic pressing (CIP) are generally used for powder compaction.[3–8]

Up to now, aqueous dispersions of ZrB_2 single powder with different dispersants were studied and 3D components were produced by freeze-form extrusion.[9,10]

This work examines the feasibility of complex shapes by slip-casting techniques of ZrB_2-based composite, containing SiC as a secondary phase and Si_3N_4 as a sintering aid. Actually, the presence of silicon carbide ensures an improvement of strength, toughness, and oxidation resistance compared with pure ZrB_2, while silicon nitride acts as the sintering aid because it removes boria, which prevents the densification.[2,11–17] The sintering process involved the well-known reaction between boria and silicon nitride, which is the main reaction occurring during heating up:[11,15–17]

$$Si_3N_4 + 2B_2O_3 \rightarrow 4BN + 3SiO_2 \qquad (1)$$

Reaction (1) is the responsible for the removal of the B_2O_3 present from ZrB_2 particle surface. For zirconium diboride, the densification without additives is very slow and is combined with an exaggerated grain growth, due to the surface oxygen contamination that retards diffusion mechanisms enhancing the evaporation/condensation kinetics.[1] The primary oxygen-bearing species, present on diborides particles, is B_2O_3, which is rapidly reduced by the addition of Si_3N_4. When almost all the B_2O_3 surrounding ZrB_2 grains have been completely depleted, pure ZrB_2 comes into contact with the silica-based liquid phase.[15]

Slip-cast green bodies were prepared and characterized after sintering at 2150°C. Sinterability and microstructure was compared with those of cold isostatic pressed materials of the same composition. Mechanical properties were also measured on slip-cast samples. In particular, preliminary tests of flexural strength up to 1500°C were performed on specimens directly produced in the shape of chamfered four-point bending bars by slip casting and without any additional machining after sintering.

Experimental Procedure

The starting composition was the following (amounts in vol%):

- ZrB_2–20 SiC–4 Si_3N_4, theoretical density: 5.40 g/cm^3.

Some characteristics of the commercial raw powders are listed in Table I.

The powder batch was ball milled for 72 h in ethanol using Si_3N_4 media. The ethanol was removed from the slurry using rotary evaporation.

Pellets with a diameter of 40 and 6.5 mm thick were uniaxially pressed and then cold isostatically pressed at 300 MPa.

To prepare slip-cast specimens, an aqueous slip of premixed powders was ball milled in a polyethylene

Table I. Main Characteristics of the Raw Starting Powders

Formula	Company	Type	Specific surface area (m^2/g)	O and free C content (wt%)
ZrB_2	H.C. Starck, ABCR (Karlsrhue, Germany)	Grade B	1	O: 1 (1.5B_2O_3), C: 0.25
α-Si_3N_4	Bayer AG (Leverkusen, Germany)	Baysinid	12.2	1.5 (2.8SiO_2)
β-SiC	H.C. Starck, ABCR	BF 12	11.6	0.9 (1.7SiO_2)

All data are from technical datasheets of the producers.

Table II. Main Characteristics of the Dispersant from Technical Datasheet of the Producer

Trade name	Supplier	Chemical nature	pH	MW (g/mol)	Solid content (wt%)	Density (g/cm^3)
Duramax D3005	Rohm & Haas (Lauterbourg, France)	Ammonium salt of acrylic homopolymer	6–7	2500	35	1.16

bottle with Si_3N_4 balls for 2 h; the slip was prepared at 38 vol% solids with Duramax D-3005 (ammonium salt of acrylic homopolymer, Rohm & Haas, Lauterbourg, France, Table II) at 2.9 wt% with respect to the mass of powder. The polyacrylate concentration (1.0 wt%) used in the preparation of the casting slips fell in an intermediate region where the zeta potential slowly decreased before the plateau, with a loss of repulsion of 6 mV with respect to the minimum value of −61.5 mV:[18] As the dispersant was a polyelectrolyte, an electrosteric stabilization occurred. Disks of 40 mm diameter were produced pouring the slip into a plastic ring on a plaster absorbent slab and different thicknesses of the green bodies were achieved. Before casting, the plaster was moistened. After 20 min, the slip-cast samples were demolded and after 20 h at room temperature they were placed into a laboratory furnace at 80°C for complete drying.

Pressureless sintering was performed at 2150°C for 2 h in a graphite furnace (Onyx Furnace 2200°C, LPA DVM, Seyssinet, France) in flowing argon. The thermal cycle consisted of a first step of binders pyrolysis at 600°C with a heating rate of 100°C/h and a holding time of 1 h; then the heating rate was increased up to 600°C/h to reach the sintering temperature of 2150°C. Green density and bulk density after sintering were measured by the geometrical method and Archimede's method, respectively.

The microstructural features were analyzed using SEM-EDS (SEM, Cambridge S360, Cambridge, U.K.; EDS, INCA Energy 300, Oxford Instruments, Oxford, U.K.) on fractured or polished sections of the sintered samples. The mean linear intercept grain size was calculated on SEM polished section micrographs with the circle method. Residual porosity and phase distribution were estimated on SEM polished section micrographs by image analysis (Image Pro Plus 6.0., Media Cybernetics, Bethesda, MD). Crystalline phases were identified by X-ray diffraction (XRD) analyses (Siemens D500, Karlsruhe, Germany).

The Vickers microhardness was measured using a Zwick 3212 tester (Ulm, Germany) with loads of 9.81 N. Net-shaped chamfered bars with a final dimension of 45 mm × 4 mm × 3 mm (length × width ×

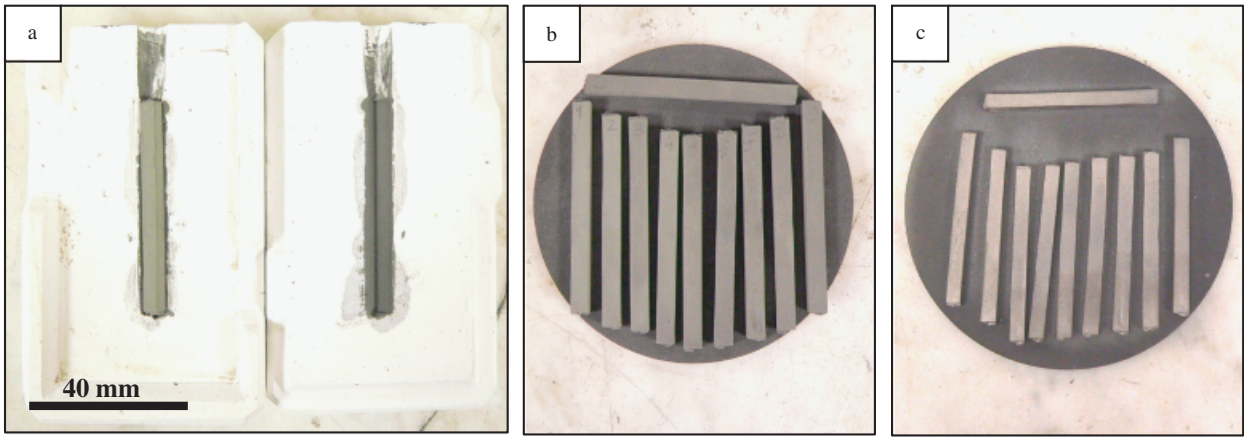

Fig. 1. Four-point bending bars: (a) demolding of the slip-cast bar from the plaster mould; (b) green bars; (c) after sintering, the bars are ready to be tested.

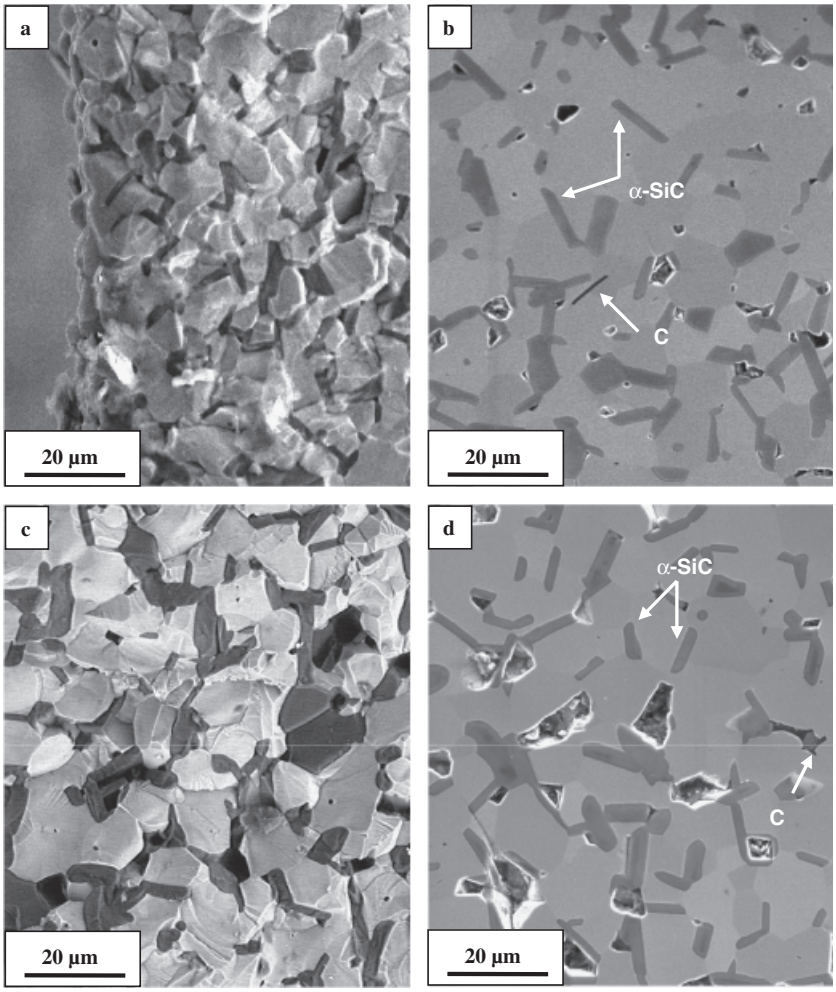

Fig. 2. Fracture and mirror-polished surfaces of slip cast (a, b) and CIP (c, d) samples after sintering a t 2150°C for 2 h in argon. In (a) the fracture near the sample surface in contact with the plaster absorbent slab. CIP, cold isostatic pressing.

thickness, respectively) were produced by slip casting in a closed plaster mold and sintering (Fig. 1) and they were used as specimens for mechanical tests without any additional machining. The Young's modulus was measured by resonant frequency specimens using a H&P gain-phase analyzer (Tokyo, Japan). The four-point flexural strength (σ) was measured from room temperature up to 1500°C in laboratory atmosphere. The flexural tests were performed on a semiarticulated silicon carbide four-point jig with a lower span of 20 mm and an upper span of 10 mm on a universal screw-type testing machine (Instron 6025, High Wycombe, U.K.). The specimens were deformed with a crosshead speed of 0.05 mm/min. For the high-temperature tests, a soaking time of 18 min was set to reach thermal equilibrium.

In order to identify the fracture origins, SEM fractography analyses were carried out on the fracture surfaces of the broken flexural specimens.

Results and Discussion

Sintering and Microstructure

The microstructures after sintering of fracture and mirror-polished surfaces of slip-cast samples are reported in Figs. 2a and b; the secondary phase, SiC, is

Table III. Density, Bulk Porosity and ZrB_2 Mean Grain Size, After Sintering of Cold Isostatic Pressed (CIP) and Slip Cast (SLIP) Samples

Sample	Green density (g/cm^3)	Green density (%)	Final thickness (mm)	Bulk density (g/cm^3)	Bulk density (%)	Residual porosity* (%)	ZrB_2 grain size* (μm)
CIP	3.25 ± 0.03	60.1	~5	5.25 ± 0.02	97.2	6.2 ± 0.3	11.8 ± 0.3
SLIP 1	2.82 ± 0.02	52.2	~3	5.38 ± 0.01	99.6	1.7 ± 0.1	8.8 ± 0.2
SLIP 2	2.82 ± 0.04	52.2	~4	5.35 ± 0.01	99.0	2.1 ± 0.1	—
SLIP 3	2.83 ± 0.01	52.4	~5	5.31 ± 0.01	98.3	2.9 ± 0.2	—

*The values were measured by image analysis.

homogenously dispersed in the entire sample. For comparison, the microstructure of samples formed by CIP are shown as well (Figs. 2c and d). Green densities and final thicknesses, bulk densities, residual porosities, and ZrB_2 grain sizes after sintering are reported in Table III.

During sintering, the weight loss was about ~3.5% for both slip-cast and cold isostatically pressed, CIP samples; weight losses were also observed for other pressureless-sintered ZrB_2- and ZrC-based materials and they were ascribed to the vaporization of volatile species such as CO and SiO.[19,20] For slip-cast samples, the linear shrinkage was homogeneous and about 18%. Instead, the diameter shrinkage of the CIP samples was ~20% while the thickness shrinkage was ~16%, because of the better particles packing achieved in this direction during the uniaxial pressing, applied before the CIP of the cylindrical samples.

The green density of slip-cast specimens was only 52%, while in the case of CIP samples it was 60%, (Table III). In the same way, during sintering, the growth of ZrB_2 grains was higher in the material from CIP. The final density of the slip-cast bodies decreased, increasing the samples thickness as reported in Table III.

In both slip-cast and CIP-sintered samples, XRD pattern showed a complete conversion of β-SiC phase into α-SiC phase as the sintering temperature is well over the β to α conversion temperature (1900°C). No Si_3N_4 traces or other phases are detected by XRD, but ZrB_2 and α-SiC.

Microstructural analyses on both slip-cast and CIP-sintered samples, evidenced in the examples shown in Figs 2 and 3, show that beside ZrB_2 and elongated α-SiC grains, traces of secondary phases such as BN, graphite, and areas rich in B_4C grains are present. These phases are not homogenously dispersed in the microstructure and no oxygen-containing phases or silica-based phases at grain boundary and/or triple point were revealed by SEM and EDS. The microstructure of the pressureless-sintered samples is very different from the microstructure of hot pressed samples having the same composition but sintered at a lower temperature, where the rounded β-SiC particles generally exhibited a clustered distribution and they were often in contact with the products of the sintering process, that is, BN, t-ZrO_2, and different glassy B–N–O–Si–Zr compounds at triple points.[11]

The residual porosity resulting from image analysis was higher with respect to the relative density estimated on the basis of the theoretical density of 5.40 g/cm^3 (Table III). This implies that the full density is expected to be higher than the theoretical one calculated by the rule of the mixture from the starting composition. Actually, in such a complex system where:

- ZrB_2 and SiC are the main components;
- Si_3N_4 is the sintering aid;
- B_2O_3, ZrO_2, and SiO_2 are originally present in the raw powders and also formed on the particles surfaces during the wet milling;[21] and
- carbon is a raw powder impurity and further carbon sources are the polyethylene bottles used during ball milling, binder, and sintering atmosphere;[6,22,23]

many reactions occurred during sintering, changing the final composition and forming new phases.

From these features, it can be hypothesized that during the sintering process the reaction between boria and silicon nitride formed boron nitride and silica, as observed previously.[11,15–17] This reaction is responsible for the removal of B_2O_3 present on the ZrB_2 particles surface. The presence of silica (deriving from SiC and Si_3N_4) helps the formation of a liquid phase as it forms a eutectic with boria and/or zirconia (which is also pres-

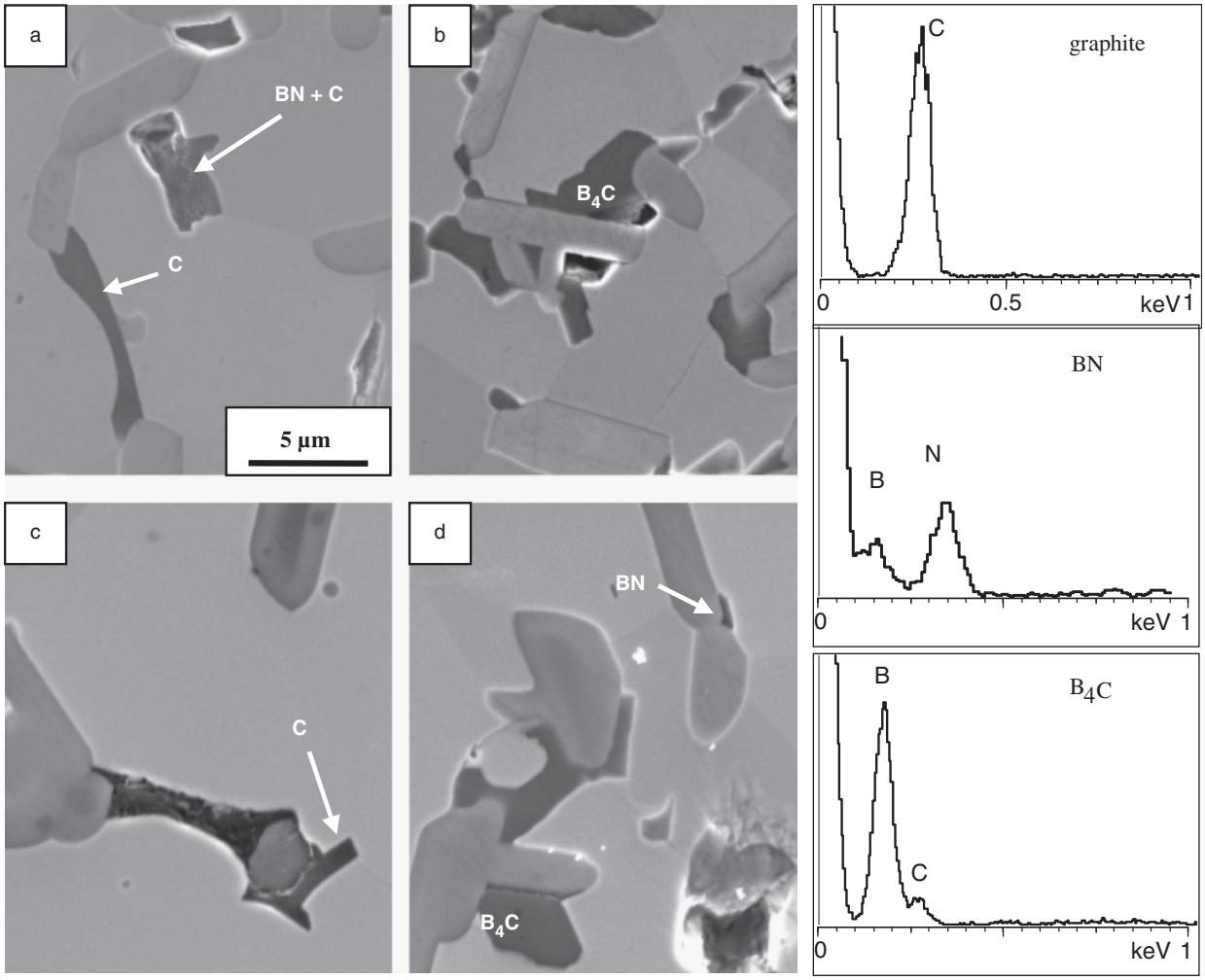

Fig. 3. Areas on mirror-polished surface of slip-cast (a, b) and CIP (c, d) sample and EDS spectra of the secondary phases: graphite, BN, and B_4C. CIP, cold isostatic pressing.

ent on ZrB_2 grains). When almost all the B_2O_3 surrounding the ZrB_2 grains have been completely depleted, pure ZrB_2 comes into contact with a mainly silica-based liquid phase.[15] Because of the high cohesive energy of group IV diborides, the liquid exudes to the triple points, associated with the consequent dewetting of the grain boundary and the main part of the boundaries between the ZrB_2 grains are flat and depleted of secondary phases.[4,8,15] As observed by Sciti *et al.*[6] comparing hot pressed and pressureless-sintered ZrB_2-based samples, the absence of silica containing tripe points in the pressureless-sintered materials is due to the carbo-reduction of the silica-based liquid phases at the sintering conditions, that is, the long soaking time at a very high temperature in a carbo-reducing atmosphere (carbon impurities and graphite furnace in flowing argon), in thin samples. A commercial software package was used to determine the equilibrium composition during sintering and the carbo-reduction of silica and boria in the temperature range 1400–2200°C at 1 bar.[25] The molar ratio of the starting compounds was taken equal to $C:SiO_2:B_2O_3 = 2:1:1$ (Fig. 4). The formation of B_4C and the weight loss of 3.5% due to the formation of volatile species, such as CO, SiO, and B_2O_3, are consistent with the thermodynamical calculations in a carbo-reductive atmosphere (Fig. 4). Therefore, sintering

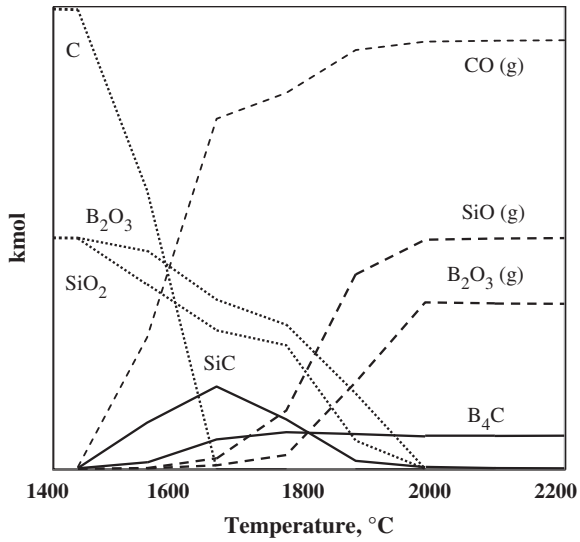

Fig. 4. Equilibrium composition calculated at a constant pressure of 1 bar, where the molar ratio of the starting compounds was taken equal to $C:SiO_2:B_2O_3 = 2:1:1$.[24]

under the experimented conditions is favored by a transient liquid phase that does not originate from silica-based grain boundary or triple-point phases, because it undergoes carbo-reduction and it is mainly transformed into a gaseous species.

Although having lower green density (Table III), slip-cast samples are denser than cold isostatic pressed ones after sintering. This could be derived from the additional amount of oxygen introduced during the ball milling in water during the preparation of the slip;[21] a greater amount of oxidized phases (SiO_2, B_2O_3) increases the liquid phase quantity favoring sintering.

Mechanical Properties

Mechanical properties measured on sintered slip-cast samples are reported in Table IV. Both hardness and Young's modulus are in line with the literature data on materials of similar composition.[11–13] However, standard deviation of hardness is quite high because of the presence of not homogeneously dispersed phases such as B_4C (36 GPa), h-BN ($\sim$280 MPa), and graphite (300 MPa).[24–27]

It has to be noted that the strength values measured on as-sintered slip cast bars increased, increasing the testing temperature from RT to 1500°C. A ZrB_2 surface layer, about 30–50 μm thick, with a porosity

Table IV. Mechanical Properties of Slip Cast As-Sintered Specimens

		σ (MPa)		
HV (GPa)	**E (GPa)**	**RT**	**1200°C**	**1500°C**
15.2 ± 0.9	437 ± 1	137 ± 2 178 ± 9*	199 ± 15	315 ± 16

*The bending tests were performed after removal of the ZrB_2 surface layer from the green specimens.
H_V, Vickers Hardness; E, Young's modulus; σ, four-point bending strength.

of 7% was detected in slip-cast bars (Fig. 5a); probably, a segregation of larger ZrB_2 grains occurred during the very early stage of slip casting in the surface in contact with the plaster mould, and, in this layer, smaller and lighter particles of SiC and/or of the sintering aid (Si_3N_4) were preset in an amount lower than those introduced in the starting composition of the slurry. This feature was not observed in the samples produced in shape of disks where no evident ZrB_2 segregation occurred and SiC is homogenously distributed through the sample (Figs. 2a and b). There is a correlation between the configuration of the plaster molds and the formation of ZrB_2 layer in the very first stages of slip casting; actually, the segregation of the ZrB_2 occurred only along the vertical walls of the plaster mold (as in the case of tested surfaces of the slip-cast bars) and it is attributed to the different electrosteric stabilities of the various components of the composite suspension.[18] The surface porous layer acted as a source of critical defects, resulting in a quite low RT strength (Table IV). For this reason, the ZrB_2 superficial layer was removed before sintering using an abrasive SiC paper (grit 1000); the resulting flexural strength was slightly higher with respect to the unmachined bars. Anyway, bulk defects due to entrapped air during slip cast acted as critical defects (Fig. 5b) as well.

At a higher temperature in the laboratory atmosphere, the oxidation of the phases constituting the composite promoted the formation of a silicatic glassy layer with a thickness ranging between 10 and 20 μm, after exposure at 1500°C (Figs. 5c and d, and EDS spectrum). This glassy phase sealed all the superficial defects increasing the strength; the higher is the testing temperature the higher is the amount of glassy phase and its effectiveness in improving strength.

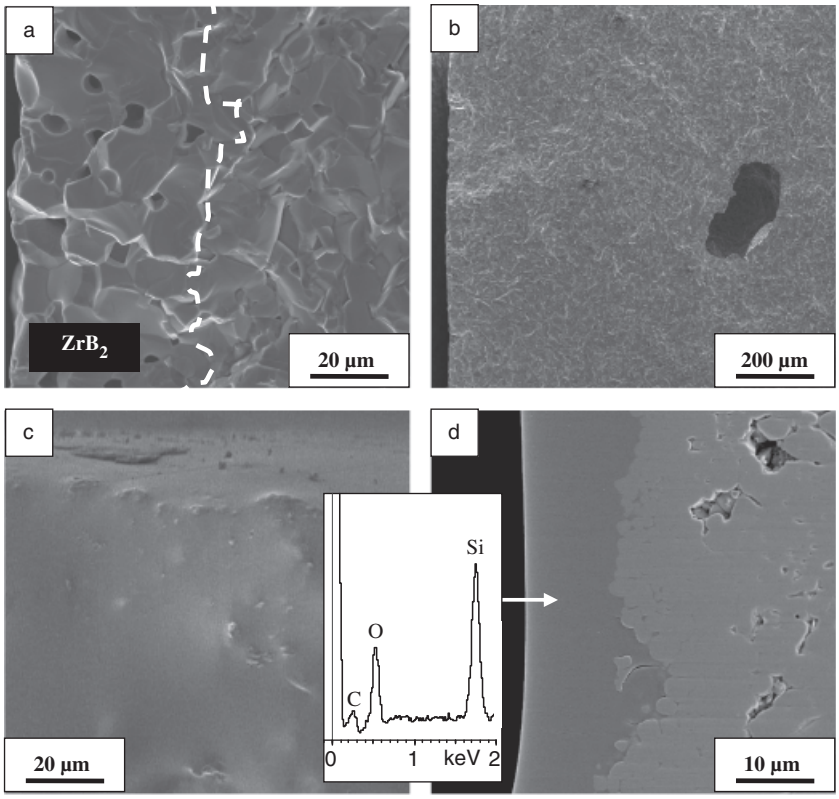

Fig. 5. SEM micrographs showing the fracture surfaces and polished cross section after strength measurements at room temperature (a, b) and at 1500°C (c, d). In (b) the fracture of a specimen where the ZrB_2 superficial layer was removed before sintering. In the box EDS spectrum of the superficial glass formed at 1500°C.

Moreover, the load-displacement curves were linear up to 1500°C (Fig. 6), this behavior being related to the absence of any possible grain boundary phases, which generally softens with consequent subcritical crack growth.

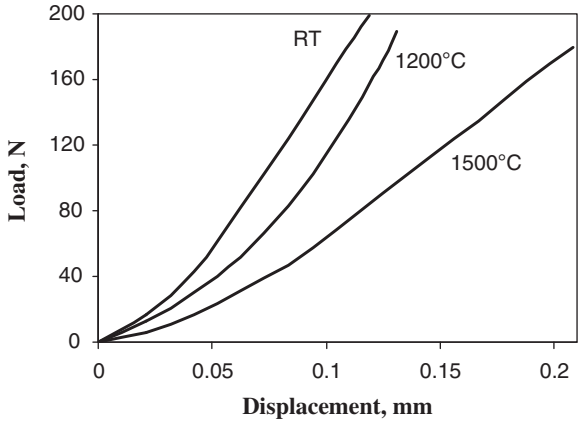

Fig. 6. Load-displacement plot of the four-point bending test at RT and high temperatures on as-sintered slip-cast bars.

Conclusion

In order to evaluate the feasibility of complex-shaped components in ZrB_2–SiC composite, the slip-casting technique was studied. The green bodies were successfully pressureless sintered at 2150°C, using silicon nitride as a sintering aid. Traces of the formation of secondary phases such as B_4C, graphite, and BN were found in all samples, while no grain boundary phases were present because of the carbo-reduction occurring during the long soaking time at the sintering temperature.

Slip casting was more effective than CIP in achieving high densities because of the additional amount of oxidized phases (SiO_2, B_2O_3, and ZrO_2, that promoted

liquid phase sintering) introduced during preparation of the slip by ball milling in water.

During slip casting of bars for flexural strength, larger ZrB_2 particles segregated at the surfaces in contact with the vertical walls of the plaster mold, forming a porous layer after sintering, which affected RT flexural strength. High-temperature flexural strength increased with the testing temperature as a glassy layer due to the oxidation reactions, sealed the superficial defects, and subcritical crack growth did not occur due to the absence of a grain boundary phase.

References

1. C. Mroz, "Zirconium Diboride," *Am. Ceram. Soc. Bull.*, 74 [6] 164–165 (1995).
2. M. M. Opeka, I. G. Talmy, E. J. Wuchina, J. A. Zaykoski, and S. J. Causey, "Mechanical, Thermal, and Oxidation Properties of Refractory Hafnium and Zirconium Compounds," *J. Eur. Ceram. Soc.*, 19 2405 (1999).
3. A. L. Chamberlain, W. G. Fahrenholtz, and G. E. Hilmas, "Pressureless Sintering of Zirconium Diboride," *J. Am. Ceram. Soc.*, 89 [2] 450 (2006).
4. A. Goldstein, Y. Geffen, and A. Goldberg, "Boron Carbide–Zirconium Diboride In Situ Composite by the Reactive Pressureless Sintering of Boron Carbide–Zirconium Mixtures," *J. Am. Ceram. Soc.*, 84 [6] 442 (2001).
5. S. G. Zhang, G. E. Hilmas, and W. G. Fahrenholtz, "Pressureless Densification of Zirconium Diboride with Boron Carbide Addition," *J. Am. Ceram. Soc.*, 89 [5] 1544 (2006).
6. D. Sciti, F. Monteverde, S. Guicciardi, and G. Pezzotti, "Microstructure and Mechanical Properties of ZrB_2–$MoSi_2$ Ceramic Composites Produced by Different Sintering Techniques," *Mater. Sci Eng.*, A 434 [1–2] 303 (2006).
7. D. Sciti, S. Guicciardi, A. Bellosi, and G. Pezzotti, "Properties of a Pressureless-Sintered ZrB_2–$MoSi_2$ Ceramic Composite," *J. Am. Ceram. Soc.*, 89 [7] 2320 (2006).
8. Y. J. Yan, Z. R. Huang, S. M. Dong, and D. L. Jiang, "Pressureless Sintering of High-Density ZrB_2–SiC Ceramic Composites," *J. Am. Ceram. Soc.*, 89 [11] 3589 (2006).
9. S. H. Lee, Y. Sakka, and Y. Kagawa, "Dispersion Behaviour of ZrB_2 Powder in Aqueous Solution," *J. Am. Ceram. Soc.*, 90 [11] 3455 (2007).
10. T. Huang, G. Hilmas, W. Fahrenholtz, and M. C. Leu, "Dispersion of Zirconium Diboride in an Aqueous, High-Solids Paste," *Int. J. Appl. Ceram. Technol.*, 4 [5] 470 (2007).
11. F. Monteverde, S. Guicciardi, and A. Bellosi, "Advances in Microstructure and Mechanical Properties of Zirconium Diboride Based Ceramics," *Mater. Sci. Eng.*, A346 [1–2] 310 (2003).
12. F. Monteverde and A. Bellosi, "Development and Characterization of Metal-Diboride-Based Composites Toughened with Ultra-Fine SiC Particulates," *Solid State Sciences*, 7 [5] 622 (2005).
13. F. Monteverde, "The Thermal Stability in Air of Hot-Pressed Diboride Matrix Composites for Uses at Ultra-High Temperatures," *Corr. Sci.*, 8 2020 (2005).
14. E. J. Opila and M. C. Halbig, "Oxidation of ZrB_2–SiC," *Ceramic Engineering and Science Proceedings*, Vol. 22 [4]. eds., M. Singh and T. Jessen. American Ceramic Society, Westerville, OH, 221, 2001.
15. F. Monteverde and A. Bellosi, "Effect of the Addition of Silicon Nitride on Sintering Behaviour and Microstructure of Zirconium Diboride," *Scr. Mater.*, 46 [3] 223–228 (2002).
16. A. Bellosi and F. Monteverde, "Ultra-Refractory Ceramics: The Use of Sintering Aids to Obtain Microstructure Control and Properties Improvement," *Euro Ceramics VIII—Part 2, Vols. 264–268, Key Engineering Materials*. eds., H. Mandal and L. Öveçoglu. Trans Tech Publications, Switzerland, 787–792, 2004.
17. I. G. Talmy, J. A. Zaykoski, and M. M. Opeka, "High-Temperature Chemistry and Oxidation of ZrB2 Ceramics Containing SiC, $TaSi_2$, Ta_5Si_3, and Si_3N_4," *J. Am. Ceram. Soc.*, 91 [7] 2250–2257 (2008).
18. V. Medri, D. Gardini, and C. Capiani, "Slip Casting of a ZrB_2–SiC composite," *J. Adv. Eng. Mater.*, in press.
19. L. Silvestroni and D. Sciti, "Effects of $MoSi_2$ Additions on the Properties of Hf– and Zr–B_2 Composites Produced by Pressureless Sintering," *Scr. Mater.*, 57 165–168 (2007).
20. L. Silvestroni, D. Sciti, J. Kling, S. Lauterbach, and H. J. Kleebe, "Sintering Mechanisms of Zirconium and Hafnium Carbide Doped with $MoSi_2$," *J. Am. Ceram Soc.*, 92 1574–1579 (2009).
21. S.-H. Lee, Y. Sakka, and Y. Kagawa, "Corrosion of ZrB_2 Powder During Wet Processing—Analysis and Control," *J. Am. Ceram. Soc.*, 91 [5] 1715–1717 (2008).
22. D. Sciti, L. Silvestroni, and M. Nygren, "Spark Plasma Sintering of Zr- and Hf-Borides with Decreasing Amounts of $MoSi_2$ as Sintering Aid," *J. Eur. Ceram. Soc.*, 28 1287–1296 (2008).
23. D. Sciti and M. Nygren, "Spark Plasma Sintering of Ultra Refractory Compounds," *J. Mater. Sci.*, 43 6414–6421 (2008).
24. A. Roine, *HSC Chemistry 5.1*, Outukumpu Research Oy, Finland.
25. P. T. B. Shaffer, "Engineering Properties of Carbides," *Engineered Materials Handbook*, Vol. 4. ed., S. J. Schneider Jr. ASM International, Materials Park, OH, 804–811, 1991.
26. A. Lipp, K. A. Schwetz, and K. Hunold, "Hexagonal Boron Nitride: Fabrication, Properties and Applications," *J. Eur. Ceram. Soc.*, 5 3–9 (1989).
27. M. Sakai and Y. Nakano, "Instrumented Pyramidal and Spherical Indentation of Polycrystalline Graphite," *J. Mater. Res.*, 19 [1] 228–236 (2004).